Projectile K-Auger-electron production by bare, one-, and two-electron ions

T. R. Dillingham, J. Newcomb,* James Hall, Philip L. Pepmiller,† and Patrick Richard
Department of Physics, Kansas State University, Manhattan, Kansas 66506
(Received 19 December 1983)

Projectile K-Auger-electron production measurements were performed for the bare, one-, and two-electron ions of C, N, O, and F incident on He, Ne, Ar, and Kr gases. The measurements were taken over an energy range of $\frac{1}{4}$ to $\frac{2}{3}$ MeV/amu using a cylindrical mirror analyzer. For the incident two-electron ions, single-electron capture to excited states of the $(1s2s)^3S$ metastable component of the incident beam was the principal mechanism giving rise to the observed K-Auger transitions. For the bare and one-electron ions, double electron capture to excited states was the dominant mechanism leading to K-Auger-electron production. In addition to Auger-spectroscopy measurements, total K-Auger production cross sections were determined as well as the partial cross sections for electron capture to specific n levels of the projectile. The n distributions were also measured for double electron capture to excited states of the bare and one-electron ions.

I. INTRODUCTION

Numerous measurements of Auger-electron production have been performed in recent years. The vast majority of these studies, however, have concentrated on collisionally produced Auger-electron emission from either the target atom or from low-charge states of the projectile ion. Thus these measurements have been used to study inner-shell vacancy production mainly via the processes of electron excitation and ionization. Until very recently, Auger-electron production has not been widely used as an investigative tool for the study of electron capture in ion-atom collisions. The review articles by Rudd and Macek,[1] Garcia *et al.*,[2] and Mathews[3] provide a very good summary of the study of Auger-electron production in addition to the general techniques involved.

In this work projectile K-Auger-electron production is studied for very highly charged incident ions in which the capture of one or more electrons to high-n levels is the dominant mechanism by which states are formed with an inner-shell vacancy. In particular, K-Auger-electron production measurements are performed for the bare, one-, and two-electron ions of C, N, O, and F incident on He, Ne, Ar, and Kr gases. Total cross sections for projectile K-Auger-electron production are presented over an energy range of $\frac{1}{4}$ to $\frac{2}{3}$ MeV/amu. Both the projectile- and target-Z dependencies of the cross sections are given in addition to the projectile charge-state dependence (for $q=Z, Z-1, Z-2$). Furthermore, partial cross sections for electron capture to specific n levels of the projectile are presented. These partial cross sections provide a rather unique set of data, since only a limited number of experimental investigations have been made which determine the distribution of final state n populations following electron capture.[4–7]

There are several advantages to studying K-vacancy production for the above-mentioned collision systems using K-Auger-electron emission techniques instead of high resolution x-ray techniques. In general, for ions with $Z \leq 20$, the fluorescence yield ω_K is much less than 1.[3,8] Thus for the collision systems of interest to this study, the decay of the excited states via K-Auger-electron emission is much more probable and less sensitive to the fluorescence yields. In addition, the low reflection efficiencies for crystal spectrometers ($\sim 10^{-5}$) make K-Auger-electron measurements much more tractable.

There are also numerous advantages in studying Auger emission by highly charged projectile ions. Previous work has shown, for example, that the collisionally produced delta-electron background decreases significantly with increasing charge state.[9,10] Thus the highly charged incident ions used in this work produce a very high peak to background ratio, which makes it easier to perform spectroscopy measurements. The use of highly charged incident ions also decreases the number of processes leading to Auger decay which can occur during the collision. Thus the interpretation of the experimental results and comparisons with theory are simplified.

II. EXPERIMENT

The experiment was performed at the James R. Macdonald Laboratory at Kansas State University using a model EN tandem Van de Graaff accelerator. The ion-induced K-Auger-electron measurements were performed by using an electrostatic cylindrical mirror analyzer. This particular type of electron spectrometer has the distinct advantage of having a very high efficiency, since almost the entire azimuthal angle 2π is accepted, while maintaining adequate resolution for the electron energies of interest. The design parameters of this particular analyzer have been presented previously by Woods *et al.*,[11] while a more general treatment of the parameters and focusing properties of the cylindrical mirror analyzer has been given by Risley[12] and Mathews.[3]

A general discussion of the experimental techniques and procedure have been presented in some detail in a previous paper.[6] In addition, the method of analysis as well

as the particular problems inherent in the study of projectile Auger-electron emission have also been given in the previous paper and so are not discussed here.

III. RESULTS AND DISCUSSION

A. Projectile *K*-Auger-electron spectra

One system of particular interest is that of an incident two-electron projectile colliding with one of the various target gases. An example of this is shown in Fig. 1, where the projectile *K*-Auger-electron spectrum for a $\frac{1}{4}$ MeV/amu F^{7+} + He collision is presented. The figure also shows the theoretical *K*-Auger transition energies of Bhalla *et al.*[13,14] and Chung.[15] It is seen that the observed electron emission comes from a three-electron (Li-like) series of autoionizing states. The formation of the observed states is possible because an appreciable fraction ($\sim$5—25 %) of the incident F^{7+} beam is not in the $(1s^2)^1S$ ground state but rather is in the metastable $(1s2s)^3S$ state. Thus the Li-like autoionizing states are formed by single-electron capture to excited states of the metastable component of the incident F^{7+} beam. A more detailed discussion of the metastable component of the incident two-electron projectiles will be given when the total Auger production cross sections are presented.

The charge-state dependence of the incident projectile has also been measured. Figure 2 shows an example of this dependence for the bare, one-, and two-electron ions of fluorine incident on Ar. The measurements were made

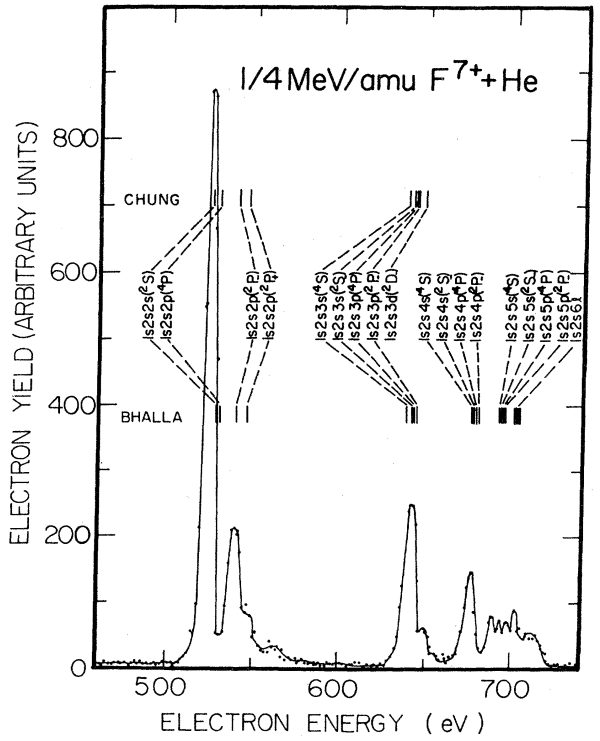

FIG. 1. Projectile *K*-Auger-electron spectrum for a $\frac{1}{4}$ MeV/amu F^{7+} + He collision is compared to theoretical Auger transition energies for $1s2snl$ Li-like states.

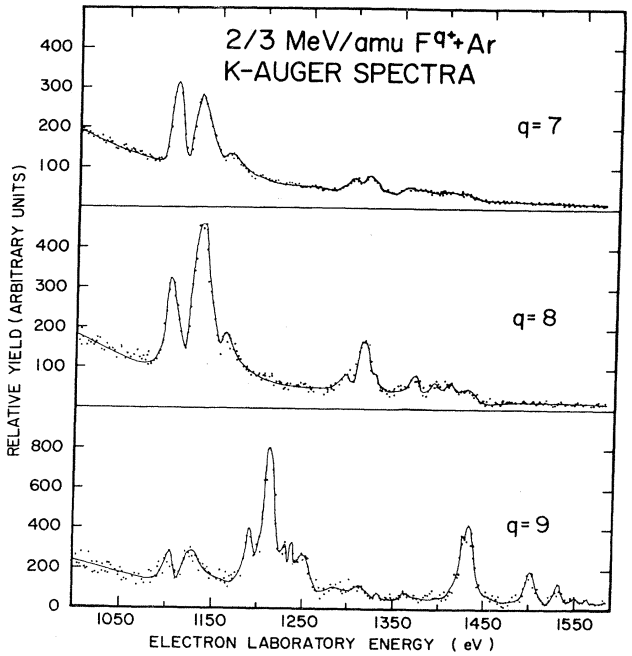

FIG. 2. Charge-state dependence of the $\frac{2}{3}$ MeV/amu F^{q+} + Ar *K*-Auger-electron spectra is shown. The spectra are presented for $q = 7$—9 in the laboratory frame of reference.

at an incident energy of $\frac{2}{3}$ MeV/amu. For the F^{7+} spectrum, the same basic features are observed (with kinematic effects), as was seen in Fig. 1 for the F^{7+} + He collision. Hence single-electron capture to an excited state of the $(1s2s)^3S$ metastable component is the mechanism responsible for the formation of the observed states. For the F^{8+} spectrum, the same three-electron (Li-like) series of states is observed with different ratios of the line intensities. Since the incident F^{8+} ion comes into the collision with a single ground-state electron, the only means by which the Li-like autoionizing states could be formed is by double electron capture to excited states of the projectile. It should be noted that the F^{8+} spectrum shows no evidence of the two-electron (He-like) hypersatellite lines (see discussion below). Hence the capture of a single electron plus $1s$ excitation of the electron already present on the incoming projectile, which would give rise to the hypersatellite lines, is not an appreciable contributing mechanism for Auger-electron production in these collision systems. For the incident F^{9+} (bare) ion, however, a different series of Auger lines is observed that is associated with the He-like hypersatellite transitions. Figure 3 shows the F^{9+} + Ar spectrum along with the theoretical hypersatellite transition energies for the $2l2l'$ states.[14,16,17] In addition, the $2snp$ transition energies, where $n \geq 3$, are given from a simple calculation using a screened hydrogenic model. The only mechanism by which these hypersatellite states can be formed is double electron capture to excited states of the projectile. In particular, not only is the capture of two electrons to the *L* shell $2l2l'$ observed, but also double capture to the $2l3l'$, $2l4l'$, ... levels, out to the series limit, is observed. It can also be seen in Fig. 2 that a small amount of the three-electron Li-like states

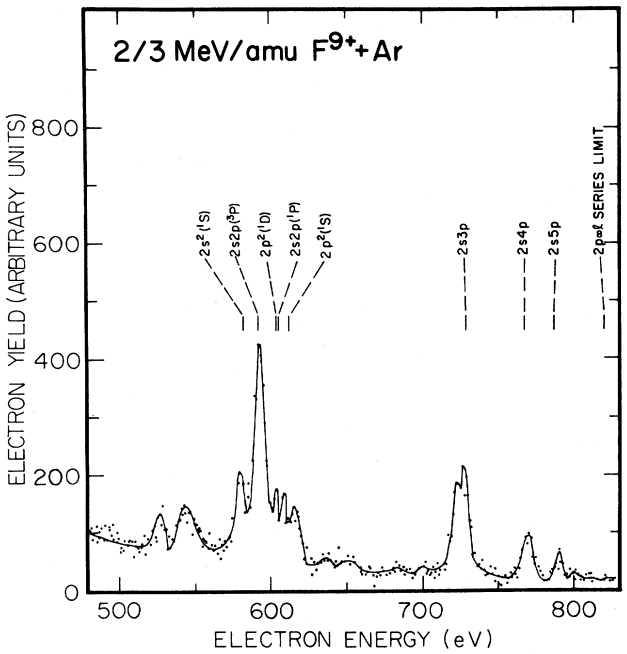

FIG. 3. K-Auger-electron spectrum for a $\frac{2}{3}$ MeV/amu F^{9+} + Ar collision is compared to theoretical Auger transition energies for several of the $2ln'l'$ hypersatellites.

are observed at ~1100 eV. These states could be formed by triple electron capture to the bare projectile. However, it is much more probable that the observed intensity is due to a small amount of F^{7+} and F^{8+} impurities in the incident F^{9+} beam formed by charge exchange upstream from the target region. It should be noted, however, that the intensity pattern for these lines is not the same as that observed for the F^{7+} and F^{8+}.

The intensity patterns of the two observed peaks (at ~1100 eV in Fig. 2) for electron capture to the $n=2$ level of F^{7+} and F^{8+} ions are given in Table I. The fraction of the intensity in each peak is given for targets of He, Ne, Ar, and Kr at incident velocities of $\frac{1}{3}$ and $\frac{2}{3}$ MeV/amu. It is seen, for example, that for the F^{7+} + He collision at $\frac{2}{3}$ MeV/amu, 63% of the observed intensity is in the first peak (^2S and ^4P states) and 37% is in the second peak (^2P states). For the F^{8+} + He collision, however, only 42% of the intensity is in the first peak while 58% is in the second. The difference in the observed intensity patterns is due to the processes by which the observed states are formed. For the incident F^{7+} ion, the observed intensity comes predominantly from the states formed by single-electron capture to the $(1s2s)^3S$ component of the beam. Hence the $(1s2s2p)^2P_+$ state, formed from the $(1s2s)^1S$ state, should not make an appreciable contribution to the observed intensity. For the incident F^{8+} ion, however, double electron capture to the $n=2$ level would produce the $(1s2s2p)^2P_+$ state in addition to the $(1s2s2p)^2P_-$ state. Thus the relative intensity for the second peak should be larger, as is observed. The intensity fractions for F^{7+} and F^{8+} on He and Ne compare favorably to previous high resolution x-ray measurements.[7,18]

The intensity fraction of the second peak also increases as the target Z is increased. The increased intensity for the higher Z targets is due to multiple capture events where additional captured electrons act only as spectator electrons. The states formed by multiple electron capture lie to the high-energy side of the second peak.[6,13] Thus the observed intensity of the second peak is increased as the target Z is increased since multiple capture events are much more probable for the higher Z targets.

The intensity fractions also show a dependence upon the incident velocity. The intensity fraction of the first peak is, in all cases, seen to decrease with increasing velocity. This velocity dependence is due to the lifetime effect of the $(1s2s2p)^4P$ state which will be discussed in detail later in the text.

The target dependence for the various incident projectiles has also been measured. Figure 4 gives an illustration of this dependence for F^{9+} ions incident on targets of He, Ne, Ar, and Kr. In this figure the previously discussed He-like hypersatellite series is clearly observed. The relative yield for K-Auger-electron production is seen to increase with increasing target Z. However, the relative capture of one electron to $n=2$ levels and the other electron to the higher n levels ($n>2$) appears to decrease as the target Z is increased. Hence for the Kr target the double electron capture occurs predominantly to the L shell ($2l2l'$ capture), while for the He target a much larger relative fraction of the double capture is to the M shell

TABLE I. The intensity fractions for electron capture to the $n=2$ level of F^{7+} and F^{8+}.

		$\frac{1}{3}$ MeV/amu		$\frac{2}{3}$ MeV/amu	
Projectile	Target	1st peak	2nd peak	1st peak	2nd peak
F^{7+}	He	0.70	0.30	0.63	0.37
F^{8+}		0.51	0.49	0.42	0.58
F^{7+}	Ne	0.58	0.42	0.53	0.47
F^{8+}		0.42	0.58	0.38	0.62
F^{7+}	Ar	0.61	0.39	0.44	0.56
F^{8+}		0.40	0.60	0.35	0.65
F^{7+}	Kr	0.52	0.48	0.43	0.57
F^{8+}		0.32	0.68	0.30	0.70

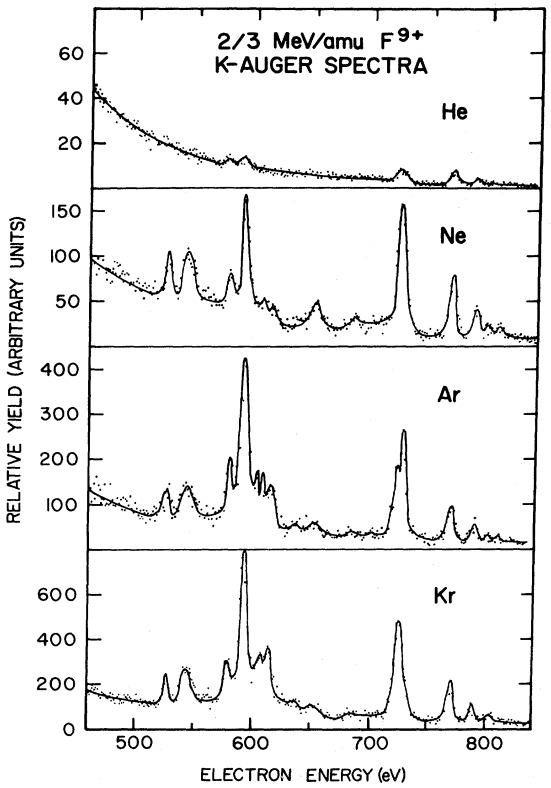

FIG. 4. Target dependence of the $\frac{2}{3}$ MeV/amu F^{9+} K-Auger-electron spectra is shown.

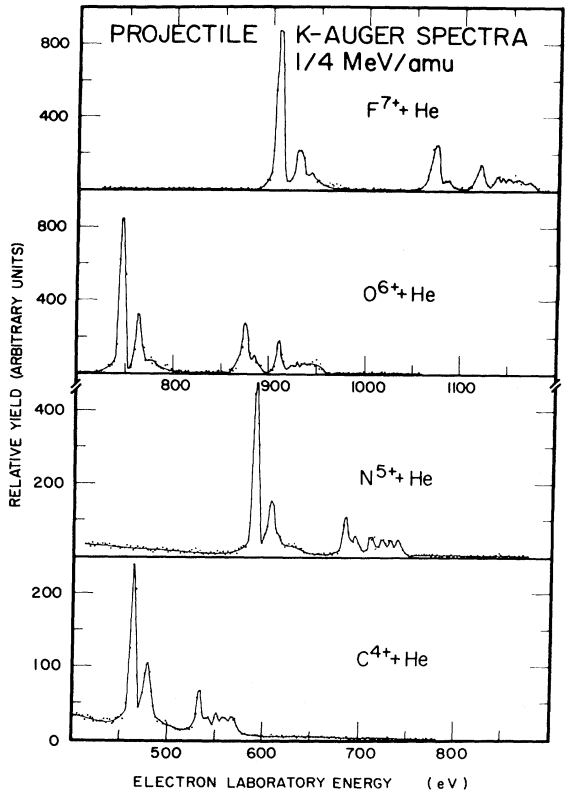

FIG. 5. Projectile-Z dependence of the K-Auger-electron spectra is shown for the various incident two-electron ions. The spectra were taken at an incident velocity of $\frac{1}{4}$ MeV/amu and are given in the laboratory frame of reference.

($2l3l'$ capture) and above. This feature will become even more apparent when the partial cross sections for electron capture are presented.

In addition to the target dependence, the projectile-Z dependence has also been measured. One example of this is given in Fig. 5 for the two-electron projectiles of C, N, O, and F incident on He. All measurements were taken at the same incident velocity. The relative yield for K-Auger-electron production is seen to increase with increasing projectile Z. Although the observed spectral features are basically the same for the various projectiles, the line energies and spacings for the observed transitions increase with increasing projectile Z due to the increased binding and energy level spacing for the higher Z ions. Finally, it can also be seen that the delta-electron background decreases for the higher Z projectiles where the observed electron energy is higher.

B. Total K-Auger-electron production cross sections

The highly charged incident projectiles used in this study are formed by passing a high velocity, low-charge-state ion through a thin carbon post-stripping foil. This method produces a distribution of charge states in addition to forming numerous excited states for a given charge state. In general, these excited states have very short lifetimes and decay to the ground state before reaching the target region. For the two-electron projectiles, however, several of these excited states are long lived and do survive to the interaction region. In particular, it can be shown that $\sim 99.6\%$ of the metastable $(1s2s)^3S$ F^{7+} state (lifetime $\tau = 277$ μsec) produced in the post-stripper foil 10 m from the target region at an energy of 9.5 MeV will reach the interaction region while only 0.6% of the $(1s2s)^1S$ state (lifetime $\tau = 198$ nsec) will survive. The fraction f_{3_S} of the $(1s2s)^3S$ component of the incident F^{7+} beam has been measured as a function of the incident energy by Terasawa *et al.*[19] The measurement involves determining the relative yield of target Ti K x rays as a function of the incoming projectile charge state. It is assumed that the $(1s^2)^1S$ component of the F^{7+} beam produces the same number of Ti K x rays as an equivalent beam of F^{q+} where $q \leq 6$. In addition, the single K vacancy bearing $(1s2s)^3S$ component of the F^{7+} beam produces the same number of Ti K x rays as an equivalent beam of F^{8+} ions. The metastable fraction f_{3_S} of the $(1s2s)^3S$ component is then given by the following expression:

$$f_{3_S} = \frac{\sigma(7+) - \sigma(6+)}{\sigma(8+) - \sigma(6+)} \approx \frac{Y(7+) - Y(6+)}{Y(8+) - Y(6+)} , \qquad (1)$$

where $\sigma(q+)$ and $Y(q+)$ represent the target K x-ray production cross section and x-ray yield, respectively.

This analysis was extended to include the other projectiles of interest to this work by utilizing the charge-state

dependence of previous x-ray measurements.[19–27] Using these x-ray measurements, the metastable fraction of the $(1s2s)^3S$ component for various projectiles is shown in Fig. 6. The fraction is given as a function of the ratio of the projectile velocity to the K-shell-electron velocity. The solid line in the figure was drawn to guide the eye. The fraction is seen to increase from 0.1 to 0.3 with increasing velocity. Since the fractions for the various projectiles all fall within the limits of error, the values from the solid line were used in the analysis of the cross sections for the incident two-electron projectiles.

Since an appreciable fraction of the incident two-electron projectiles are in the $(1s2s)^3S$ metastable state, single-electron capture to this state can result in a K-Auger transition. The incident two-electron ions in the $(1s^2)^1S$ ground state could also give rise to K-Auger transitions, but only by a two-step process. This process would involve the simultaneous capture of an electron to an excited state plus K-shell excitation and is expected to be much less probable than single capture to the metastable state.

The total cross sections for projectile K-Auger-electron production by F^{7+} ions incident on He and Ne targets are shown in Fig. 7. The total cross sections have been adjusted by the fraction of the $(1s2s)^3S$ metastable component as given in Fig. 6. The cross sections are given as a function of projectile energy and are compared to a theoretical Oppenheimer-Brinkman-Kramers[28] (OBK) calculation for electron capture. The OBK calculation is well known to lie above experiment by as much as an order of magnitude,[29,30] and was normalized to the $\frac{1}{3}$ MeV/amu F^{7+} data. Appropriate screening parameters[31–33] for spectator electrons have been included in this calculation. It can be seen that the OBK calculation gives general agreement for the energy dependence of the capture cross section over this energy range, although the experimental result lies above theory for the lowest energy. However, the agreement appears somewhat better for the He target than for the Ne target.

The projectile-Z dependence of the total K-Auger-electron production cross sections for the various two-electron incident ions is shown in Fig. 8. All measure-

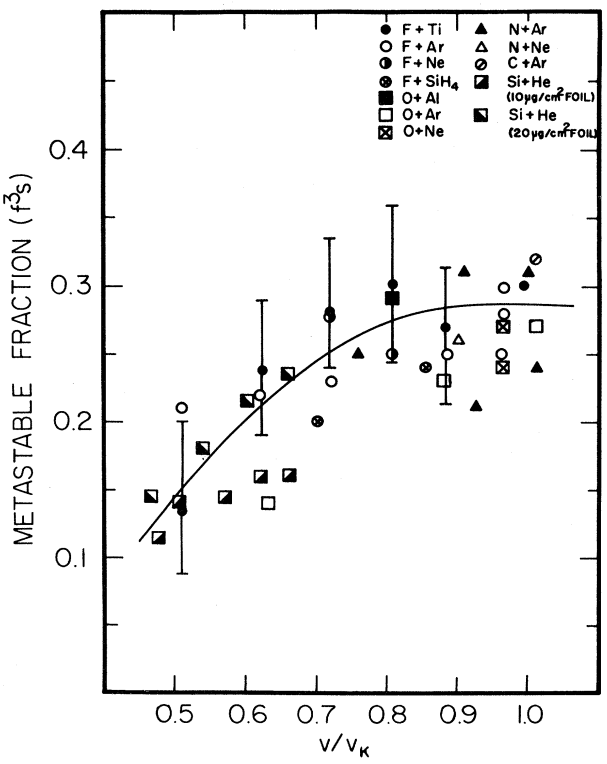

FIG. 6. The fraction f_{3_S} of the $(1s2s)^3S$ component is shown for various incident two-electron projectiles as a function of the ratio of the projectile velocity to the K-shell-electron velocity. The solid line is drawn to guide the eye and used in the analysis of the cross sections.

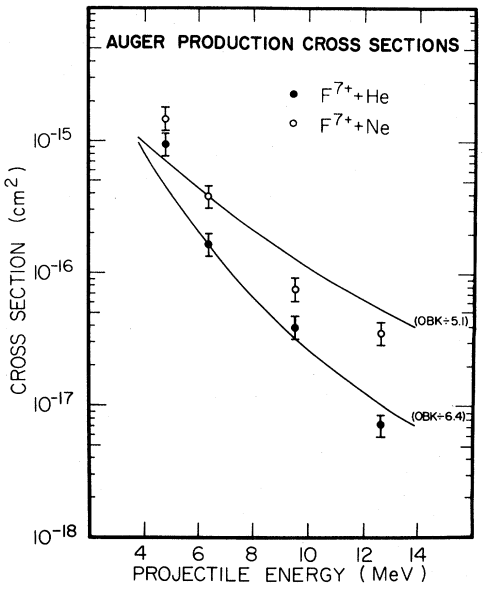

FIG. 7. Energy dependence of the total K-Auger-electron production cross sections for F^{7+} + He and Ne is compared to a theoretical OBK calculation. The calculation is normalized to the 6.33 MeV F^{7+} data.

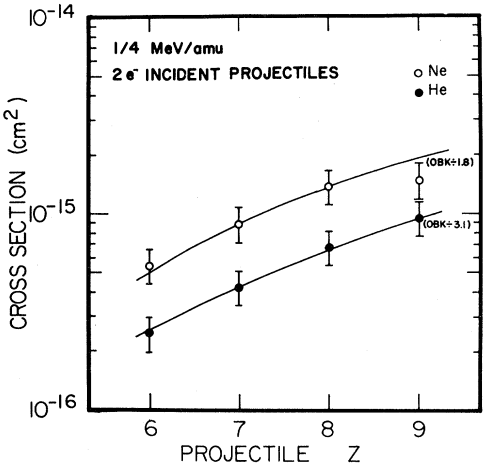

FIG. 8. Projectile-Z dependence of the total K-Auger-electron production cross sections is shown for the various two-electron ions at an incident velocity of $\frac{1}{4}$ MeV/amu. The results are compared to an OBK calculation normalized to the N^{5+} result.

ments were made at the same projectile velocity of $\frac{1}{4}$ MeV/amu. The results are compared to an OBK calculation normalized to the N^{5+} experimental measurements. It can be seen from the figure that the cross sections increase with increasing projectile Z and that the projectile-Z dependence given by the normalized OBK calculation is in good agreement with the experimental results.

Total K-Auger-electron production cross sections were also measured for the one-electron F^{8+} ions incident on He, Ne, Ar, and Kr gases. The results are given in Fig. 9 as a function of projectile energy. The curves in the figure are drawn to guide the eye. As was discussed in the preceding section, the mechanism giving rise to K-Auger-electron production for an incident one-electron ion is double electron capture to excited states of the projectile. It can be seen from the figure that the cross section for this process falls off with energy much more rapidly for the lower Z targets. In addition, it is seen that the cross sections with a Ne target cross over those with an Ar target at the lower energies. This indicates that for the near-symmetric collision system, the matching of projectile and target energy levels plays an important role in the charge-exchange process.[34–36] Although some work, both theoretical and experimental, has been performed for double K-shell to K-shell electron transfer,[37] a theory for double electron capture to excited states of the projectile has not been established in the literature.

The projectile-Z dependence of the total K-Auger-electron production cross sections for the incident one-electron ions is shown in Fig. 10. All measurements were made at the same incident velocity of $\frac{1}{3}$ MeV/amu. The solid lines are drawn to guide the eye. The cross sections, which represent double electron capture to excited states of the one-electron ions, increase with increasing projectile Z and exhibit the same basic systematic behavior as that seen with the incident two-electron ions as given in Fig. 8.

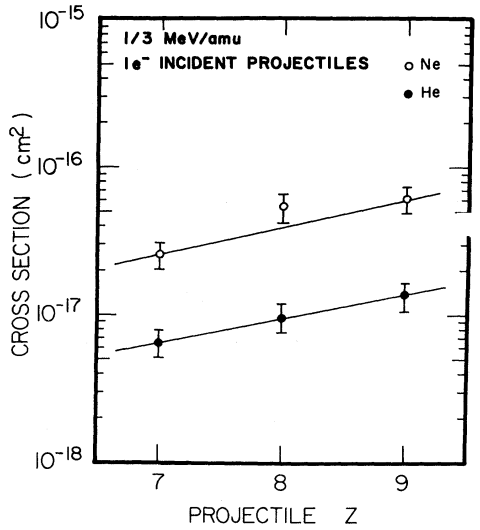

FIG. 10. Projectile-Z dependence of the total K-Auger-electron production cross sections is shown for the various one-electron ions at an incident velocity of $\frac{1}{3}$ MeV/amu. The solid lines are drawn to guide the eye.

The dependence of the total K-Auger-electron production cross section on the incident projectile charge state is shown in Fig. 11. The measurements were taken at the same projectile velocity of $\frac{2}{3}$ MeV/amu using He, Ne, Ar, and Kr target gases. For the incident fluorine ion, the cross section is observed to decrease in magnitude as the charge state is increased from 7 to 8. As discussed previously, the mechanism giving rise to K-Auger-electron pro-

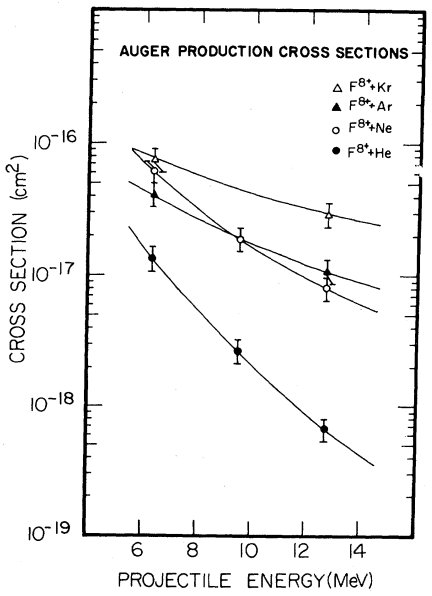

FIG. 9. Energy dependence of the total K-Auger-electron production cross sections is shown for F^{8+} incident on He, Ne, Ar, and Kr gases. The solid lines are drawn to guide the eye.

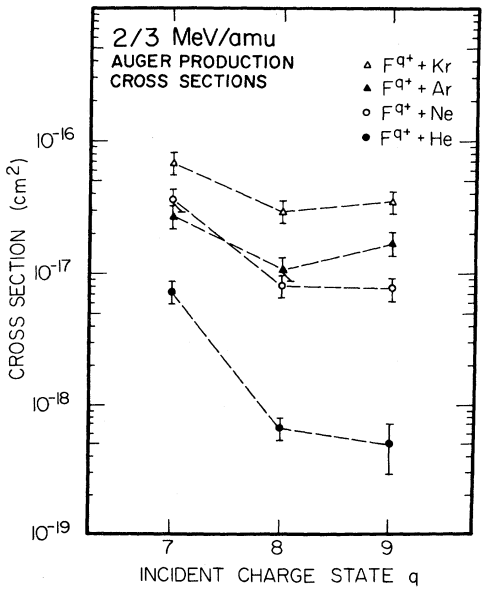

FIG. 11. Charge-state dependence of the total K-Auger-electron production cross sections is shown for $\frac{2}{3}$ MeV/amu F^{q+} ($q=7,8,9$) incident on He, Ne, Ar, and Kr gases. The dashed lines are drawn to guide the eye.

duction for the F^{7+} ion is single-electron capture to the $(1s2s)^3S$ metastable component of the beam. For the F^{8+} ion, however, double electron capture to excited states leads to K-Auger-electron emission. Since the double capture process should be less probable than the single capture process, the cross section should decrease for the F^{8+} ion, as is observed. For the Kr and Ar targets, and within the error bars for the He and Ne targets, the cross section increases for the bare F^{9+} projectile. The mechanism giving rise to K—Auger-electron emission for an incident F^{9+} ion is also double electron capture to excited states. However, with a F^{8+} projectile, the electron already present on the ion would provide some screening during the collision. Hence the F^{8+} cross section would be expected to be lower than the F^{9+}, as is observed. Figure 11 also shows the target dependence of the cross section. It is observed that for the F^{7+} + Ne collision, the cross section is above that with an Ar target, indicating once again the importance of energy-level matching for the near-symmetric collision system.[34–36]

C. n distributions for electron capture

Numerous studies of electron capture to excited states from x-ray production measurements (mainly in poor resolution) have been performed in recent years.[38,39] However, only a limited number of measurements have been made which determine the distribution of final-state n populations following electron capture.[4–7] In the present work not only are total cross sections measured for the electron-capture process, but also partial cross sections for electron capture to specific n levels are determined from Auger production measurements.

The OBK approximation predicts, for sufficiently high velocities or sufficiently high n levels, that the electron capture to excited states will behave as a $1/n^3$ function.[28] Figure 12 shows the partial cross sections for single-electron capture to the $n=2$, 3, and 4 levels, and the sum of all levels ≥ 5 for a F^{7+} ion incident on He and Ne targets. The measurements were taken at a projectile velocity of $\frac{1}{3}$ MeV/amu and are compared to a $1/n^3$ function normalized to the $n=3$ level. It is clear from the figure that the partial cross sections do indeed show a $1/n^3$ dependence. However, Fig. 12 also shows the OBK calculation normalized to the $n=3$ level. It is evident from this comparison that the OBK approximation does not have a $1/n^3$ dependence at these projectile velocities and thus does not agree with the experimental results for the n dependence of the electron capture. Therefore, either the projectile velocity is not sufficiently large for the OBK approximation to give a $1/n^3$ dependence for electron capture to the lower levels, or some other processes not included are affecting the n distributions.

One process that could account for some of the discrepancies between the experimentally observed n dependence for electron capture and the theoretical prediction is the effect of cascading. This process can occur when an electron is captured to a high n level of the projectile, and rather than undergoing deexcitation via the Auger process, decays to a lower level through x-ray emission. Thus the electron can cascade down to a lower energy level, and if the ion subsequently decays via a K-Auger transition, the observed K-Auger-electron yield for the lower n levels will be enhanced. Since the time spent in the viewing region of the analyzer, and hence the time allowed for the electron to cascade to a lower energy level, is ~250 psec for a $\frac{1}{3}$ MeV/amu projectile for example, cascading may be an important effect. This problem has been investigated to some degree in a previous paper[6] using a hydrogenic model and assuming only $E1$ x-ray transitions as possible decay channels. This investigation showed that although the agreement between experiment and the theoretical OBK calculation is improved by including cascading effects, it does not account for all of the discrepancy. However, additional detailed analysis of the cascading process should provide more insight into this problem and is a subject for future investigation.

In addition to the effects of cascading, the lifetime effects for individual states may also contribute to the discrepancies between experiment and theory for the n dependence of electron capture. If the excited state created by electron capture has a liftetime on the order of or longer than the length of time the ion spends in the viewing region of the analyzer, only a fraction of the intensity of that state will be observed. In general, the lifetimes of the excited states created by electron capture are relatively short ($<10^{-14}$ sec).[8] An exception to this is the lithium-like $(1s2s2p)^4P$ state. The lifetimes of this state for the projectiles of interest are given in Table II.[40] In addition, this table contains the fraction R of the measured K-Auger-electron intensity to the total intensity for the projectiles of interest. The measured fraction was determined

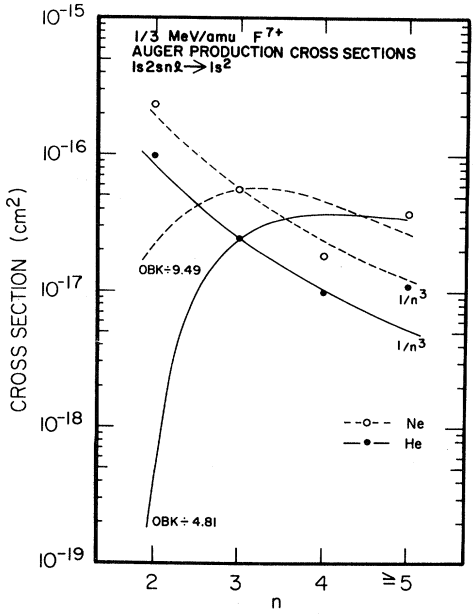

FIG. 12. n dependence of the partial capture cross sections is shown for $\frac{1}{3}$ MeV/amu F^{7+} incident on He and Ne. The capture to level ≥ 5 represents a summation of all higher n levels for the experimental result. The partial cross sections are compared to a $1/n^3$ function and an OBK calculation normalized to the $n=3$ result.

TABLE II. Lifetimes and fractions of measured intensities, R, for the Li-like $(1s2s2p)^4P$ states.

State	Z	Lifetimes (sec)	R
$(1s2s2p)^4P_{1/2}$	6	1.60×10^{-7}	0.02
	7	3.68×10^{-8}	0.10
	8	1.07×10^{-8}	0.30
	9	3.57×10^{-9}	0.66
$(1s2s2p)^4P_{3/2}$	6	6.37×10^{-8}	0.06
	7	1.45×10^{-8}	0.23
	8	4.20×10^{-9}	0.60
	9	1.39×10^{-9}	0.94
$(1s2s2p)^4P_{5/2}$	6	8.85×10^{-8}	0.04
	7	4.27×10^{-8}	0.09
	8	2.30×10^{-8}	0.15
	9	1.28×10^{-8}	0.26

in Table II for an incident projectile velocity of $\frac{1}{3}$ MeV/amu by the following expression:[41]

$$R=\int_{X_0}^{X_0+X_1}\frac{(1-e^{-\lambda X})}{X_1}dX\,, \tag{2}$$

where X_0 is the distance from the entrance aperture of the interaction region to the start of the analyzer viewing region, X_1 is the length of the analyzer viewing region, and $\lambda(=1/v\tau)$ is the decay constant expressed in units of inverse length for a projectile of velocity v and a state having a lifetime τ. It can be seen from Table II that the observed fraction of the substates of the $(1s2s2p)^4P$ state ranges from 0.02 to 0.94 and is largely dependent on the projectile Z. It should also be noted, however, that since the decay constant λ is a function of projectile velocity, the observed fraction also contains some velocity dependence. Hence for the higher velocity projectiles, an even smaller fraction of the $(1s2p2p)^4P$ state will be observed.

The above-mentioned lifetime effect applies not only to the partial cross sections for electron capture to the $n=2$ level, but also to the total cross sections as well. However, difficulties are encountered when trying to correct the measured intensities for this effect. As seen in Fig. 1, the experimental resolution was such that the $(1s2p2p)^4P$ multiplet could not be resolved from the $(1s2s^2)^2S$ multiplet. Thus the contribution of the $(1s2s2p)^4P$ multiplet cannot be determined experimentally, although a statistical analysis could be used to estimate the contribution. Lifetime effect corrections to the partial cross section for electron capture to the $n=2$ level would tend, however, to increase the cross section. It can be seen from Fig. 12 that an increase in the cross section for the $n=2$ level would not improve the agreement between experiment and theory but, in fact, would diminish the agreement.

Partial cross sections, representing single-electron capture to different n levels, are given for various incident two-electron ions in Fig. 13. Shown are the partial cross sections for capture to the $n=2$, 3, and 4 levels, and the sum of all levels ≥ 5. The measurements were taken at a

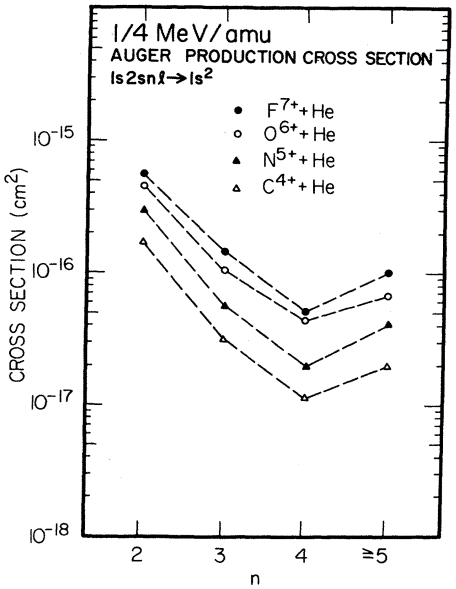

FIG. 13. n dependence of the partial capture cross sections is shown for the two-electron ions of C, N, O, and F at an incident velocity of $\frac{1}{4}$ MeV/amu. The capture to level $n\geq 5$ represents a summation of all higher n levels. The dashed lines are drawn to guide the eye.

projectile velocity of $\frac{1}{4}$ MeV/amu. The lines in the figure are drawn to guide the eye. The partial cross sections for single-electron capture follow a $1/n^3$ dependence as discussed previously.

Partial cross sections can also be determined for the incident one-electron ions. An example of this is shown in Fig. 14 for $\frac{1}{3}$ MeV/amu F^{8+} ions incident on He, Ne, Ar,

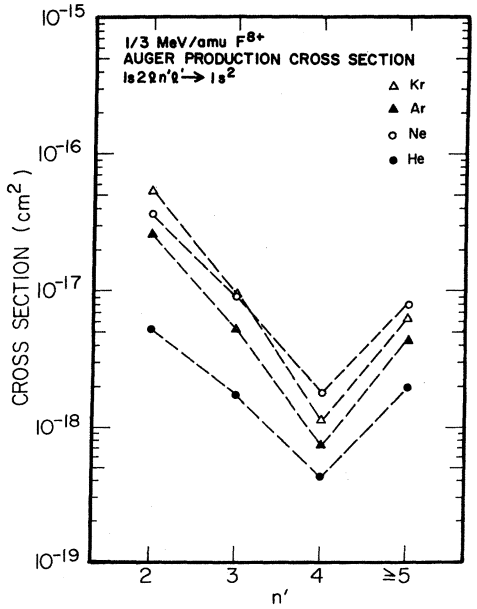

FIG. 14. n dependence of the partial capture cross sections is shown for $\frac{1}{3}$ MeV/amu F^{8+} incident on He, Ne, Ar, and Kr. The partial cross sections have been summed for the capture to levels ≥ 5. The dashed lines are drawn to guide the eye.

and Kr gases. The dashed lines in the figure are drawn to guide the eye. These partial cross sections represent double electron capture where one electron is captured to the $n=2$ level and the other is captured to the n' level where $n' \geq 2$. The partial cross sections have been summed for all levels ≥ 5.

The partial cross sections for $\frac{2}{3}$ MeV/amu F^{9+} ions incident on He, Ne, Ar, and Kr gases are shown in Fig. 15. The dashed lines in the figure are drawn to guide the eye. For the incident bare fluorine projectile, the partial cross sections also represent double electron capture where one electron is captured to the $n=2$ level and the other is captured to an n' level ≥ 2. Hence the measured intensity comes from the He-like hypersatellite transitions. It is clear from this figure that the partial cross sections are very dependent upon the choice of the target. As discussed previously (Fig. 4), it is apparent that the relative capture of electrons to the higher n' levels (>2) decreases dramatically as the target Z is increased. Hence for the He target a relatively large amount of the electron capture is to the higher n' levels. In contrast, for the Kr target a relatively larger amount of the capture occurs to the lower n' levels of the projectile. When the electron binding energies of the target are compared to the energy levels of the F^{9+} projectile, it is observed, for example, that the $M_{II,III}$ levels of the Kr match relatively closely the $n=2$ level of the F^{9+} projectile. For the He target, however, the binding energy of the K-shell electrons match closely to the $n=7$ level of the F^{9+} ion. Thus, the binding energies of the target electrons appear to play a significant role in determining into what level of the projectile the electron will be captured.

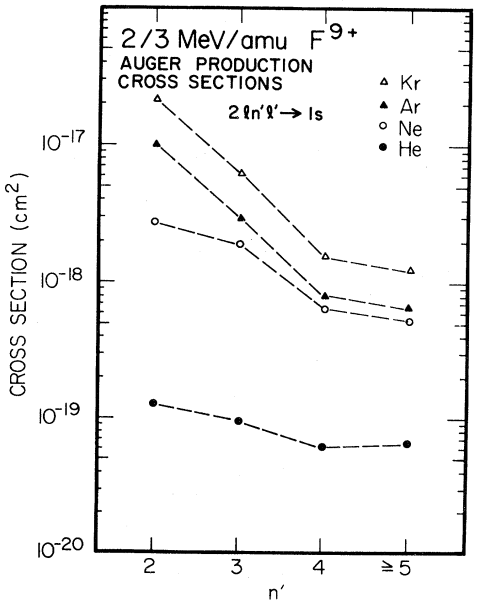

FIG. 15. n dependence of the partial capture cross sections is shown for $\frac{2}{3}$ MeV/amu F^{9+} incident on He, Ne, Ar, and Kr. The partial cross sections have been summed for the capture to levels ≥ 5. The dashed lines are drawn to guide the eye.

IV. SUMMARY

Measurements of projectile K-Auger-electron production were performed for the bare, one-, and two-electron ions, for C, N, O, and F incident on He, Ne, Ar, and Kr gases. For the incident two-electron ions, the electron emission was observed to come from a three-electron (Li-like) series of autoionizing states. These states are formed by single-electron capture to excited states of the $(1s2s)^3S$ metastable component of the incident two-electron beam. The total cross sections for this process fall off by several orders of magnitude with increasing projectile energy and are in general agreement with the energy dependence as given by a normalized OBK calculation.[28] In addition to total cross sections, partial cross sections for single-electron capture to a level n were also measured. The partial cross sections for single-electron capture were seen to follow a $1/n^3$ dependence. Furthermore, a comparison between the observed n dependence of electron capture and that given by an OBK calculation (which does not have a $1/n^3$ dependence at the measured velocities) showed large disagreement. However, a previous study[6] indicates that when the effects due to cascading are included, the agreement is improved. This effect, however, does not account for all of the discrepancy between experiment and theory for the observed n distributions. More recent theoretical studies[42–44] have improved on the OBK approximation for electron capture, but, for the capture of loosely bound electrons to excited states of the projectile, such calculations are not easily accessible.

For the incident one-electron ions, the same series of Li-like autoionizing states was observed as was seen with the incident two-electron ions. For the one-electron ions, however, these Li-like states can only be formed by double electron capture to excited states. In the observed spectra, no evidence was seen of the two-electron (He-like) hypersatellite lines, indicating that $1s$ excitation plus electron capture to excited states was not an appreciable contributing mechanism for K-Auger-electron production. Both the target dependence and projectile-Z dependence were presented for the total cross sections. In addition, partial cross sections were presented which represent double electron capture where one electron is captured to the $n=2$ level and the other is captured to a level n' where $n' \geq 2$.

For the incident bare fluorine projectiles, a different series of Auger lines associated with the He-like hypersatellite transitions were observed. These lines have not been previously observed in any projectile Auger spectrum. Only recently have these lines been observed in neon target Auger spectra from coincidence measurements.[45] For the bare fluorine projectiles, however, the observed states are formed by double electron capture, where one electron is captured to the $n=2$ level and the other is captured to a level n' where $n' \geq 2$. In addition to total K-Auger production cross sections, partial cross sections for capture to various n levels were presented for He, Ne, Ar, and Kr targets. The observed n distributions were largely dependent upon the target. For the He target, for example, a relatively large amount of the capture was to the higher n levels. In contrast, a relatively large

amount of the capture was to the lower n levels for the Kr target. The observed n distributions for the various targets showed a correlation with the matching of projectile and target energy levels.

ACKNOWLEDGMENTS

This work was supported by the Division of Chemical Sciences, U.S. Department of Energy.

*Present address: National Space Technology Laboratories, Code 245, Naval Ocean Research and Development Activity, U.S. Department of the Navy, NSTL Station, MS 39529.

†Present address: Oak Ridge National Laboratory, Oak Ridge, TN 37830.

[1]M. E. Rudd and J. H. Macek, Case Stud. At. Phys. 3, 2 (1972).

[2]J. D. Garcia, R. J. Fortner, and T. M. Kavanagh, Rev. Mod. Phys. 45, 111 (1973).

[3]D. L. Mathews, in *Methods of Experimental Physics,* edited by P. Richard (Academic, New York, 1980), Vol. 17, pp. 433–527.

[4]R. Bruch, L. J. Dube, E. Träbert, P. H. Heckmann, B. Raith, and K. Brand, J. Phys. B 15, L857 (1982).

[5]P. Hvelplund, E. Samsøe, L. H. Anderson, H. K. Haugen, and H. Knudson, Phys. Scr. T3, 176 (1983).

[6]J. Newcomb, T. R. Dillingham, J. Hall, S. L. Varghese, P. L. Pepmiller, and P. Richard, Phys. Rev. A 29, 82 (1984).

[7]H. Tawara, P. Richard, K. A. Jamison, T. J. Gray, J. Newcomb, and C. Schmiedekamp, Phys. Rev. A 19, 1960 (1979).

[8]T. W. Tunnell, C. Can, and C. P. Bhalla, IEEE Trans. Nucl. Sci. 26, 1124 (1979).

[9]J. Newcomb, P. Richard, J. M. Hall, T. R. Dillingham, P. L. Pepmiller, and S. L. Varghese, *International Conference on X-Ray and Atomic Inner-Shell Physics, Programs and Abstracts* (University of Oregon, Eugene, 1982), Vol. 2, p. 190.

[10]J. Newcomb, T. R. Dillingham, J. Hall, S. L. Varghese, P. L. Pepmiller, and P. Richard, Phys. Rev. A (to be published).

[11]C. W. Woods, R. L. Kaufman, K. A. Jamison, N. Stolterfoht, and P. Richard, Phys. Rev. A 13, 1358 (1976).

[12]J. S. Risley, Rev. Sci. Instrum. 43, 95 (1972).

[13]C. Can, T. W. Tunnell, and C. P. Bhalla, J. Electron Spectrosc. Relat. Phenom. 27, 75 (1982).

[14]C. P. Bhalla and T. W. Tunnell (private communication).

[15]K. T. Chung (private communication).

[16]P. L. Pepmiller, P. Richard, J. Newcomb, J. M. Hall, and T. R. Dillingham, Phys. Rev. A (to be published).

[17]C. Can, M. S. thesis, Kansas State University, 1981.

[18]P. L. Pepmiller and P. Richard, Phys. Rev. A 26, 786 (1982).

[19]M. Terasawa, T. J. Gray, S. Hagmann, J. Hall, J. Newcomb, P. Pepmiller, and P. Richard, Phys. Rev. A 27, 2868 (1983).

[20]S. J. Czuchlewski, J. R. Macdonald, and L. D. Ellsworth, Phys. Rev. A 11, 1108 (1975).

[21]U. Schiebel, B. L. Doyle, J. R. Macdonald, and L. D. Ellsworth, Phys. Rev. A 16, 1089 (1977).

[22]L. M. Winters, J. R. Macdonald, M. D. Brown, T. Chiao, L. D. Ellsworth, and W. W. Pettus, Phys. Rev. A 8, 1835 (1973).

[23]H. Tawara, P. Richard, T. J. Gray, P. Pepmiller, J. R. Macdonald, and R. Dillingham, Phys. Rev. A 19, 2131 (1979).

[24]G. Gealy, M. S. thesis, Kansas State University, 1978.

[25]J. R. Macdonald, L. Winters, M. D. Brown, T. Chiao, and L. D. Ellsworth, Phys. Rev. Lett. 29, 1291 (1972).

[26]J. R. Macdonald and J. Guffy (unpublished).

[27]C. W. Woods, R. L. Kaufman, K. A. Jamison, C. L. Cocke, and P. Richard, J. Phys. B. 7, L474 (1974).

[28]M. R. C. McDowell and J. P. Coleman, *Introduction to the Theory of Ion-Atom Collisions* (North-Holland, Amsterdam, 1970), Sec. 8.2.

[29]J. H. McGuire and C. L. Cocke (unpublished).

[30]A. M. Halpern and J. Law, Phys. Rev. Lett. 31, 4 (1973).

[31]H. Eyring, J. Walter, and G. Kimball, *Quantum Chemistry* (Wiley, London, 1944), p. 162.

[32]J. M. Hansteen, O. M. Johnsen, and L. Kochbach, At. Data Nucl. Data Tables 15, 305 (1975).

[33]R. E. Olson and A. Salop, Phys. Rev. A 16, 531 (1977).

[34]T. J. Gray, C. L. Cocke, and R. K. Gardner, Phys. Rev. A 16, 1907 (1977).

[35]C. L. Cocke, S. L. Varghese, and B. Curnutte, Phys. Rev. A 15, 874 (1977).

[36]T. M. Kavanagh, M. E. Cunningham, R. C. Der, R. J. Fortner, J. M. Khan, E. J. Zaharis, and J. D. Garcia, Phys. Rev. Lett. 25, 1473 (1970).

[37]J. Hall, P. Richard, T. J. Gray, C. D. Lin, K. Jones, B. Johnson, and D. Gregory, Phys. Rev. A 24, 2416 (1981).

[38]J. A. Guffey, L. D. Ellsworth, and J. R. Macdonald, Phys. Rev. A 15, 1863 (1977).

[39]J. R. Macdonald, in *Atomic Inner-Shell Processes,* edited by B. Craseman (Academic, New York, 1975), Vol. 1, pp. 74–152.

[40]T. R. Dillingham, M. S. thesis, Kansas State University, 1980.

[41]F. Hopkins, R. L. Kauffman, C. W. Woods, and P. Richard, Phys. Rev. A 9, 2413 (1974).

[42]W. Fritsch and C. D. Lin, J. Phys. B 15, 1255 (1982).

[43]J. Macek and S. Alston, Phys. Rev. A 26, 250 (1982).

[44]P. R. Simony and J. H. McGuire, J. Phys. B 14, L737 (1981).

[45]S. Hagmann, C. L. Cocke, P. Richard, A. Skutlartz, H. Schmidt-Böcking, and R. Schuch, Bull. Am. Phys. Soc. 28, 816 (1983).